

A 6-17 μm tunable and high-pulse-energy far-infrared laser based on a $BaGa_4Se_7$ optical parametric oscillator

Kejun Wang(王柯君), Hui Kong(孔辉), Xiaoxia Li(李晓霞), Dongbo Lv(吕东博), and Peng Xie(谢鹏)
Citation: Chin. Phys. B, 2026, 35 (**1**): 014210. DOI: 10.1088/1674-1056/adf82d
http://cpb.iphy.ac.cn; http://iopscience.iop.org/cpb

What follows is a list of articles you may be interested in

Optically pumped wavelength-tunable lasing from a GaN beam cavity with an integrated Joule heater pivoted on Si

Feifei Qin(秦飞飞), Yang Sun(孙阳), Ying Yang(杨颖), Xin Li(李欣), Xu Wang(王旭), Junfeng Lu(卢俊峰), Yongjin Wang(王永进), and Gangyi Zhu(朱刚毅)
Chin. Phys. B, 2023, 32 (**5**): 054210. DOI: 10.1088/1674-1056/acc05e

Design of three-dimensional imaging lidar optical system for large field of view scanning

Qing-Yan Li(李青岩), Yu Zhang(张雨), Shi-Yu Yan(闫诗雨),Bin Zhang(张斌), and Chun-Hui Wang(王春晖)
Chin. Phys. B, 2022, 31 (**7**): 074201. DOI: 10.1088/1674-1056/ac4a67

Continuous-wave Nd:$KGd(WO_4)_2$ single-longitudinal-mode laser

Rui-Jun Lan(兰瑞君), Guang-Hua Liu(刘广华), Huan-Huan Min(闵欢欢), Tong-Yu Dai(戴通宇), Ying-Jie Shen(申英杰), Peng-Hua Mu(穆鹏华), Cheng Ren(任承), De-Zhong Cao(曹德忠), and Xavier Mateos
Chin. Phys. B, 2021, 30 (**8**): 084201. DOI: 10.1088/1674-1056/abea99

A scanning distortion correction method based on *X*- *Y* galvanometer Lidar system

Bao-Ling Qi(漆保凌), Chun-Hui Wang(王春晖), Dong-Bing Guo(郭东兵), and Bin Zhang(张斌)
Chin. Phys. B, 2021, 30 (**4**): 044206. DOI: 10.1088/1674-1056/abcf42

Dynamic measurement of beam divergence angle of different fields of view of scanning lidar

Qing-Yan Li(李青岩), Shi-Yu Yan(闫诗雨), Bin Zhang(张斌), and Chun-Hui Wang(王春晖)
Chin. Phys. B, 2021, 30 (**2**): 024205. DOI: 10.1088/1674-1056/abc155

A 6–17 μm tunable and high-pulse-energy far-infrared laser based on a $BaGa_4Se_7$ optical parametric oscillator

Kejun Wang(王柯君)[1,2,3], Hui Kong(孔辉)[1,2,3,†], Xiaoxia Li(李晓霞)[1,2,3,‡], Dongbo Lv(吕东博)[1,2,3], and Peng Xie(谢鹏)[1,2,3]

[1] *State Key Laboratory of Pulsed Power Laser Technology, College of Electronic Engineering, National University of Defense Technology, Hefei* 230037, *China*
[2] *Advanced Laser Technology Laboratory of Anhui Province, Hefei* 230037, *China*
[3] *Nanhu Laser Laboratory, National University of Defense Technology, Changsha* 410073, *China*

(Received 1 July 2025; revised manuscript received 24 July 2025; accepted manuscript online 6 August 2025)

Tunable mid-infrared and far-infrared laser output was demonstrated based on $BaGa_4Se_7$ crystals and an optical parametric oscillator (OPO). With a 1.06 μm Nd:YAG laser and a double-pass singly resonant OPO cavity, a laser energy output of 2.2 mJ at 10 μm was obtained. By tuning the angle and temperature, a tunable laser output covering the wavelength range from 6 μm to 17 μm was obtained with a tuning precision better than 3 nm. The corresponding optical-to-optical conversion efficiency was 2.8%, and the slope efficiency was 4.4%. The damage effect of the output laser on detectors was also investigated, and point damage to the detector occurred at an output energy of 16.4 μJ. The laser system has the advantages of miniaturization, a wide tuning range, high energy and high tuning resolution. Its broadband laser characteristics make it highly valuable for applications in atmospheric detection, infrared spectroscopy and electro-optical countermeasures.

Keywords: $BaGa_4Se_7$, tunable laser, optical parametric oscillator, far-infrared laser

PACS: 42.70.Mp, 42.65.Yj, 42.15.Eq

DOI: 10.1088/1674-1056/adf82d **CSTR:** 32038.14.CPB.adf82d

1. Introduction

Lasers, characterized by high coherence, brightness and directionality, have found increasingly widespread applications in scientific research, industrial production and military fields.[1] Mid-infrared (MIR) lasers in particular are in high demand for applications in electro-optical countermeasures, environmental monitoring, medical treatment and molecular spectroscopy due to their unique wavelength tunability.[2,3]

There are two main methods for generating MIR lasers: direct laser generation and nonlinear frequency conversion. Although direct laser generation can produce MIR output, the output wavelength and beam quality are often limited by the intrinsic properties of the lasing medium, resulting in a narrow tunable range that cannot cover a broad MIR spectrum.[4] Therefore, we adopted the nonlinear frequency conversion method for generating MIR lasers to achieve a wide tunable laser output.

Among nonlinear frequency conversion methods, the method based on an optical parametric oscillator (OPO) that incorporates a resonant cavity shows significantly higher intracavity intensity and conversion efficiency compared with other methods. This method offers unique advantages in generating high-power MIR broadband lasers,[5] characterized as fully solid state and widely tunable, making it of significant research interest. Nonlinear crystals are key to this technology.[6] Among MIR nonlinear crystals, $BaGa_4Se_7$ (BGSe) stands out due to its large nonlinear coefficient (d_{11} = 24.3 pm·V^{-1}), broad transmission range (0.47–18 μm) and high damage threshold (557 MW·cm^{-2}).[7] The combination of BGSe crystals and OPO technology for generating MIR broadband lasers offers many advantages, such as wide tuning, full solid-state operation, high beam quality and high conversion efficiency, making it an important research area in MIR laser generation.[8]

Yao *et al.* first synthesized $BaGa_4Se_7$ crystals in 2010, and achieved optical parametric amplification in 2013, with an output wavelength of 3–5 μm.[9,10] When the pump light had a single-pulse energy of 9.1 mJ, an idler light output of 830 μJ at 3.9 μm was obtained, with a peak power of 27 MW. In 2016, Kostyukova *et al.* first demonstrated a BGSe OPO with an idler wavelength range of 2.7–17 μm.[11] In 2019, Kang *et al.* achieved a high-conversion-efficiency BGSe OPO using a double-pass pumped singly resonant OPO (DSRO) cavity.[12] With a pump energy of 13.5 mJ, an idler light output of 1.03 mJ at 4.25 μm was obtained, corresponding to an optical-to-optical conversion efficiency of 7.6% and a slope efficiency of 12%. In 2021, Bian *et al.* designed a BGSe OPO based on temperature tuning. By adjusting the temperature from 30 °C to 140 °C, a laser output in the wavelength range of 3.637–3.989 μm was achieved with a tuning precision of

†Corresponding author. E-mail: konghui17@nudt.edu.cn
‡Corresponding author. E-mail: Lixiaoxia17@nudt.edu.cn

© 2026 Chinese Physical Society and IOP Publishing Ltd. All rights, including for text and data mining, AI training, and similar technologies, are reserved.

3.2 nm·°C^{-1}.[13] In 2024, Liu *et al.* designed a high-peak-power, wide-tunable-range long-wave infrared OPO based on BGSe crystals.[14] Pumped by a 1.06 μm Nd:YAG laser, it achieved a peak power of 0.15 MW at 9.8 μm with a pulse width of 5.0 ns. At 11.0 μm, a high beam quality was obtained with $M_x^2 = 4.1$ and $M_y^2 = 3.3$. By rotating the BGSe crystal, a wide tuning range of 6.7–13.9 μm was realized. In 2025, Hu *et al.* used a 2.1 μm laser to pump a BGSe OPO, obtaining femtosecond laser output in the 7–15 μm wavelength range and an energy of 52 μJ at 9.7 μm.[15]

Although previous research has demonstrated generation of laser output in the MIR range using BGSe OPOs, the characterization of output energy and tuning precision in the far-infrared (FIR) range needs to be improved. Our work addresses this gap by achieving high-energy, wide-band and high-precision laser output in the FIR range using a 1064 nm pump source and BGSe crystals, covering the wavelength range from 6 μm to 17 μm with a single-pulse energy of 2.2 mJ at 10.2 μm and temperature tuning precision better than 3 nm.

2. Experiments

To achieve laser output in the 6–17 μm band, a laser experimental system was constructed as shown in Fig. 1. A mature 1.064 μm Nd:YAG laser (SL800) was used as the pump source, with a pulse width of 13 ns, a repetition rate of 1 Hz and a beam diameter of 8 mm. Two pinhole apertures, D1 and D2, were used to adjust the light in the system, where D1 was for adjusting the telescope system and D2 for the OPO system. In order to reduce the spot radius of the pump source from 4 mm to 2 mm, a telescope system (T) composed of a combination of convex and concave lenses, was employed.

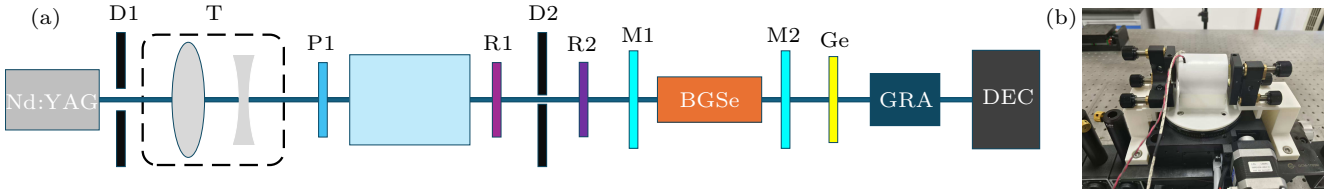


Fig. 1. Experimental device: (a) schematic diagram and (b) picture of the physical OPO.

In selection of the OPO cavity, a simple and highly efficient DSRO cavity was considered, composed of a nonlinear crystal and two OPO cavity mirrors, M1 and M2, at the two ends of the cavity. Mirror M1 has high transmission ($T > 90\%$) at 1.06 μm, high reflection ($R > 85\%$) at 1.13–1.36 μm and high transmission ($T > 80\%$) at 5–17 μm. Mirror M2 has high reflection ($R > 98\%$) at 1.06 μm, high reflection ($R > 90\%$) at 1.13–1.36 μm and high transmission ($T > 80\%$) at 5–17 μm. When the pump light passes through the OPO cavity, the mirrors reflect the generated signal light and the pump light back into the optical path while outputting the desired idler light and forming the DSRO cavity. The BGSe crystal in the cavity has dimensions of 10 mm×10 mm×40 mm (with a light path length of 40 mm) and a cutting angle of (42.5°, 0°). It was polished to achieve high transmittance for the signal light (1.13–1.36 μm), the pump light (1.06 μm) and the idler light (5–17 μm). The optical isolator, composed of a polarizer (P), a Faraday rotator (FR) and a 45° rotator (R1), was designed to prevent the reflecting laser from entering the pump source and causing damage.

A 90° rotator (R2) was placed between the optical isolator and the OPO system because the pump light is horizontally polarized before entering the OPO. After passing through the rotator, the angle of the crystal can be changed by rotating the crystal horizontally on the rotation stage, otherwise it would be necessary to rotate the crystal vertically for wavelength tuning, which is difficult to achieve and prone to crystal slippage.

Figure 1(b) shows a physical picture of the optical resonator, in which the BGSe crystal was placed in an electric rotation platform with an embedded groove. The angle of the crystal can be tuned by remotely controlling the rotation platform via a computer. Temperature tuning of the crystal can be achieved by adding a temperature-controlled furnace. The OPO cavity mirrors were mounted on adjustment stands (Zolix OMHS25-BS), which were fixed on the optical platform with 3D-printed connectors. Compared with ordinary 3D mirror adjustment stands, these stands occupy a shorter length in the optical path, thus forming a short-cavity OPO system (with a cavity length of 55 mm). This device reduces the pump threshold of the BGSe crystal while increasing the conversion efficiency of the pump light to the idler light.

A Ge plate was placed behind the OPO to absorb all laser light below 1.7 μm, filtering out the remaining pump and signal light that passes through the OPO system and improving the accuracy of the experimental data. A grating spectrometer (GRA; Zolix Omni 300) was placed after the Ge plate for spectral analysis, and the transmission wavelength of the spectrometer can be adjusted via a computer. A photoelectric detector (DEC; DEC-M204) was placed at the output port of the spectrometer and connected to an oscilloscope (OSC; DSOX3024T). The wavelength measurement section consists of a GRA, a computer, a MIR detector (DEC) and an OSC. The transmission wavelength of the spectrometer was controlled by the computer. The output wavelength of the idler light can be determined by observing the OSC waveform and the transmission wavelength of the spectrometer.

In this experiment, to achieve wide-band laser output it is necessary to perform angle tuning on the crystal based on its nonlinear characteristics. The crystal was placed on an electric rotation platform and the angle of the BGSe crystal was tuned by adjusting the rotation stage via a computer. At the same time, a Thorlabs ES111C energy meter was used to measure the output energy of the laser device at normal incidence (with the end face normal and the incident light at 0°) and at other angles.

3. Methods

BGSe crystals obey the Sellmeier equation at room temperature; this was revised by Kato in 2023 as follows:[16]

$$\begin{cases} n_x^2 = 6.72431 + \dfrac{0.26375}{\lambda^2 - 0.04248} + \dfrac{608.63}{\lambda^2 - 756.87}, \\ n_y^2 = 6.86603 + \dfrac{0.26816}{\lambda^2 - 0.04259} + \dfrac{682.97}{\lambda^2 - 781.78}, \\ n_z^2 = 7.16709 + \dfrac{0.32681}{\lambda^2 - 0.06973} + \dfrac{731.86}{\lambda^2 - 790.16}, \\ \quad 0.901 \le \lambda \le 13.703, \end{cases} \tag{1}$$

where n_x, n_y and n_z represent the refractive indices of the crystal along the x, y, z principal axes, respectively, and λ is the wavelength of the laser.

As BGSe is a biaxial crystal, two angles (θ, φ) are used to denote the direction of the light beam, where θ is the angle between the light beam and the z-axis and φ is the angle between the plane formed by the light beam and the z-axis and the x-axis.

The phase mismatch can be given by

$$\Delta k = 2\pi \left| \frac{n_{e2}^{\lambda_p}}{\lambda_p} - \frac{n_{e2}^{\lambda_s}}{\lambda_s} - \frac{n_{e1}^{\lambda_i}}{\lambda_i} \right|. \tag{2}$$

When $\Delta k = 0$, phase matching is achieved. The phase matching curve at $\varphi = 0°$ for BGSe crystals under type I phase matching is shown in Fig. 2

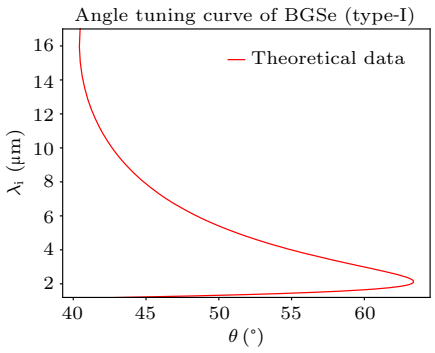


Fig. 2. Phase matching curve of BGSe ($\varphi = 0°$).

From Fig. 2 it can be seen that by controlling the electric rotation platform with a computer to adjust the θ angle of the crystal, the laser output covering the MIR and FIR bands can theoretically be obtained.

Studies have shown that the refractive index of the crystal is also affected by temperature. Kato *et al.* measured the fundamental wavelength at which the crystal achieved maximum second-harmonic efficiency at different temperatures and provided the Sellmeier equation for the crystal under the influence of temperature[17]

$$\begin{cases} \dfrac{dn_x}{dT} = \left(\dfrac{6.0868}{\lambda^3} - \dfrac{12.6368}{\lambda^2} + \dfrac{10.5624}{\lambda} + 1.9583 \right) \\ \qquad \times 10^{-5}\ (°C^{-1}), \\ \dfrac{dn_y}{dT} = \left(\dfrac{6.3935}{\lambda^3} - \dfrac{13.1762}{\lambda^2} + \dfrac{10.8950}{\lambda} + 2.4079 \right) \\ \qquad \times 10^{-5}\ (°C^{-1}), \\ \dfrac{dn_z}{dT} = \left(\dfrac{6.3141}{\lambda^3} - \dfrac{13.0790}{\lambda^2} + \dfrac{10.8486}{\lambda} + 2.0758 \right) \\ \qquad \times 10^{-5}\ (°C^{-1}). \end{cases} \tag{3}$$

Therefore, by tuning the temperature and angle, it is theoretically possible to achieve laser output covering the MIR and FIR spectral regions. In this paper, we used a 1.06 μm laser as the pump source to excite a BGSe crystal with a cutting angle of (42.5°, 0°). When the phase-matching conditions were satisfied, stable laser output in the 6–17 μm band was achieved by tuning the temperature and angle. This scheme is theoretically consistent with the nonlinear characteristics of the crystal and is highly feasible.

4. Results and discussion

4.1. BGSe OPO laser output characteristics

To achieve high-energy laser output, the beam expander (T) was removed from the experimental setup and pump light with a spot radius of 4 mm was directly used to excite the BGSe crystal. Power scaling is straightforwardly achieved by using a stronger pump in BGSe with an available large aperture size. To measure the output characteristics of the BGSe OPO, the pump voltage on the pump source was changed under normal incidence conditions and the relationship between the idler light energy and the corresponding pump energy was obtained, as shown in Fig. 3. It should be pointed out that the values for idler light energy in Fig. 3 came from the measured data after considering a Ge plate transmittance of 56% in the corresponding wavelength range.

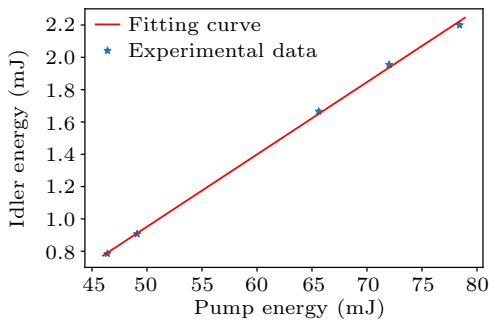


Fig. 3. Laser output characteristic (without a beam expander).

The results show that the device can output a maximum idler light energy of 2.20 mJ with a slope efficiency of 4.4% and an optical-to-optical conversion efficiency of 2.8%.

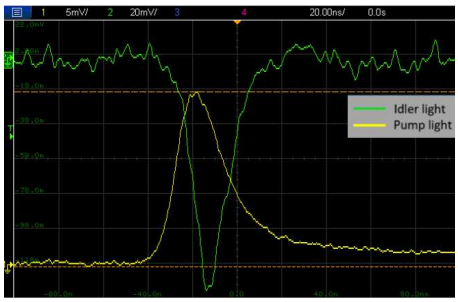


Fig. 4. Temporal profile of the pump wave and idler wave.

To observe the temporal correlation between the pump and idler pulses, we recorded the residual pump light and the idler light separately with two detectors; the result is shown in Fig. 4. The yellow trace corresponds to the pump pulse while the green trace represents the idler. The idler pulse is slightly delayed in time relative to the pump, and the full widths at half maximum (FWHMs) are 25 ns and 17 ns, respectively. The broader spectral width of the pump pulse is attributed to partial energy conversion into the idler.

4.2. Angle tuning and temperature tuning of BGSe

Angle tuning of the BGSe OPO is crucial for achieving laser output covering the MIR and FIR spectral regions. The angle between the normal to the BGSe crystal end faces and the incident light was adjusted using an electric rotation stage, and the output wavelengths at different angles were measured to further investigate the nonlinear characteristics of the crystal. The relationship between the output wavelength and the incident angle is shown in Fig. 5(a). In this figure, the experimental data (as shown by the scatter plot) are in good agreement with the theoretical data (as indicated by the Sellmeier equation of Kato).

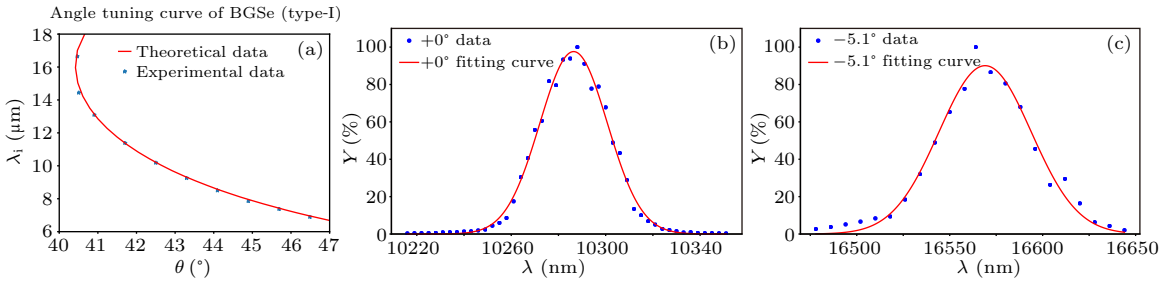


Fig. 5. Angle tuning of BGSe: (a) tuning curve of BGSe; (b) spectrum at 10 μm. (c) spectrum at 16.5 μm.

Table 1. Angle tuning output results for BGSe crystal.

Rotation stage angle (°)	Θ (°)	Output wavelength of idler (nm)
–5.1	40.465	16478–16650
–5	40.505	16164–16298
–4	40.904	13730–13840
–2	41.702	11444–11580
0	42.5	10216–10354
+2	43.298	9248–9362
+4	44.096	8504–8608
+6	44.894	7842–7956
+8	45.692	7312–7402
+10	46.49	6858–6916
+12	47.288	6434–6468
+13	47.687	6242–6274

The rotation stage changes by $\Delta\theta = 2°$ each time. For the type I matched BGSe crystal (42.5°, 0°), the refractive index of the pump light in the crystal, calculated from its Sellmeier equation, is $n_p = 2.507$. Therefore, for each rotation of the stage, the internal angle of the crystal changes by $\Delta\theta' = \Delta\theta/n_p = 0.798°$. The Gauss fitting spectra of the idler are shown in Figs. 5(b) and 5(c). When the rotation stage angles were 0° and −5.1°, we obtained laser output at wavelengths of 10 μm and 16.5 μm, respectively. The FWHMs of the idler are 33 nm and 58 nm. By changing the rotation stage angle of the BGSe crystal and simultaneously employing an OSC and a grating spectrometer, we acquired the angle tuning data of the idler. The specific angle tuning results are shown in Table 1.

As can be seen from Table 1, the spectral width gradually increases from the MIR to the FIR region. For an idler light output above 10 μm, the corresponding output spectral range is greater than 100 nm, which is considered broadband laser output and is highly desirable for specific applications.

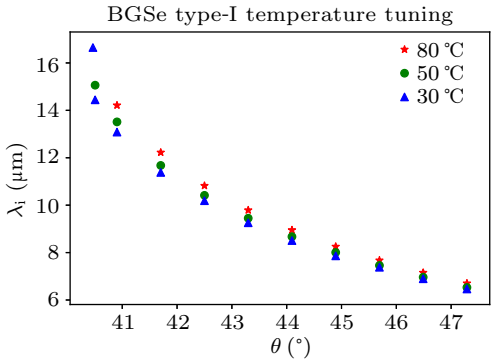


Fig. 6. Temperature tuning curve of BGSe.

To further investigate the nonlinear characteristics of the crystal, the crystal was placed in a temperature-controlled furnace and temperature tuning was achieved by setting different

temperature gradients. The output wavelengths of the crystal at different temperatures and angles θ are shown in Fig. 6.

By tuning temperature, we achieved MIR and FIR laser outputs covering the 6.2–16.7 μm band. As shown in Fig. 6, the output wavelength gradually shifts towards the FIR region as the temperature increases, which is in good agreement with the theory. However, near 16 μm, the corresponding output wavelength of the crystal could not be measured at some temperatures. This is likely because the longer the output wavelength, the higher the pump threshold. If the pump energy continuously increases, the OPO coating layer is prone to damage (the damage threshold is approximately 20 MW·cm^{-2}). The wavelength tuning precision values at corresponding rotation angles of $-4°$, $-2°$, $0°$, $+2°$, $+4°$, $+6°$, $+8°$, $+10°$, $+12°$ and $+13°$ are shown in Table 2. The tuning resolution is better than 3 nm in the FIR band and better than 0.5 nm in the MIR band.

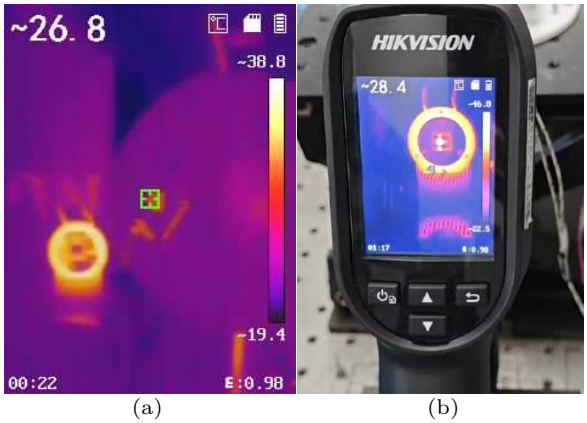
Table 2. Temperature tuning output results for BGSe crystal.

Rotation stage angle (°)	Peak wavelength at 30 °C (nm)	Peak wavelength at 50 °C (nm)	Peak wavelength at 80 °C (nm)	Tuning resolution (nm)
–4	14544	15061	–	2.58
–2	13083	13513	14213	2.26
0	11382	11676	12224	1.684
+2	10189	10414	10822	1.266
+4	9258	9450	9789	1.062
+6	8508	8601	8950	0.844
+8	7862	8006	8255	0.786
+10	7381	7457	7673	0.584
+12	6896	6962	7154	0.516
+13	6465	6529	6704	0.478

4.3. Characteristics of FIR laser damage

To investigate the damage characteristics of the 10 μm band laser output from the OPO under normal incidence conditions, we placed a thermal imager (HIKVISION DS-TPH10-3AUF) at the end of the optical path. The detector is an uncooled vanadium oxide microbolometer and the detector resolution is 160×120.

To facilitate the observation of differences in imaging quality, we set the temperature-controlled furnace to 50 °C and placed it in the optical path. By observing the imaging of the temperature-controlled furnace by the thermal imager we assessed the effects of laser damage, as shown in Fig. 7(a). To protect the back side of the detector we added a Ge plate to prevent excessive incident energy.



(a) (b)

Fig. 7. Illustration of laser damage on the detector: (a) thermal imager displaying images; (b) diagram of the laser damage effect.

When the pump voltage increased to the critical point, as shown in Fig. 7(b), a bright spot appeared on the right side of the screen, and after the laser was turned off a dark spot appeared on the screen. This indicates that irreversible point damage occurred on the thermal imager detector.

As shown in Fig. 8, based on the previously measured data it can be inferred that the output energy corresponding to this critical point is 29 μJ. However, since a Ge plate was added at the output end, which has a transmittance of 56% for this wavelength band, the actual laser energy reaching the detector was 16.4 μJ.

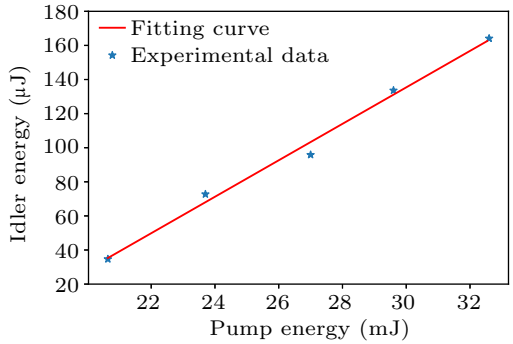


Fig. 8. BGSe OPO laser output characteristics (with beam expander).

From the experiment it can be seen that the 10 μm laser output from the OPO has a certain damaging effect on this type of detector. By increasing the pump voltage, a higher output energy can be obtained, which can make this laser suitable for application to other laser countermeasure scenarios.

5. Conclusion

The signal and idler light wavelengths of the BGSe OPO after temperature control are quite stable, and the theoretical and experimental data are in good agreement. By tuning the

angle of the BGSe crystal using an electric rotation stage, continuous wavelength variation was achieved, yielding MIR and FIR laser output covering the 6–17 μm band with a maximum single-pulse energy of 2.2 mJ. This represents broad wavelength adjustment and high tuning resolution. Further temperature tuning of the crystal using a temperature-controlled furnace ultimately achieved laser output with a tuning precision better than 3 nm. The linear OPO-based optical system is simple in structure and highly practical, offering reference significance for miniaturization and full solidification of MIR and FIR lasers. The angle tuning operation of this system is convenient, and the electric rotation stage controlled by a computer is suitable for rapid angle tuning within a wide tuning range. Meanwhile, we observed the damage effect of the FIR laser output on the detector, achieving point damage to the detector at 16.4 μJ. This further illustrates is application scenarios and has certain reference significance for laser countermeasures and other fields. In addition, we can increase the laser repetition rate by tuning the frequency of the pump light. Our present system delivers 1–10 Hz pulses. To date, most reported BGSe-based laser sources have been operated at repetition rates below 1 kHz.[18] The crystal's thermal conductivity (0.56–0.74 $W{\cdot}m^{-1}{\cdot}K^{-1}$) is the main limiting factor. To achieve high repetition, a more advanced cooling device is needed.[19]

Our laser solution based on a BGSe OPO can provide some theoretical and experimental guidance and reference for the design of miniaturized, applied MIR and FIR lasers with good tunability. During our research on the nonlinear characteristics of BGSe crystals we found that there is a theoretical possibility of achieving ultra-broadband laser output. As a next step, we plan to design an ultra-broadband laser to cover the entire MIR and FIR spectral regions.

Acknowledgement

This work was supported by Independent Innovation Science Foundation of National University of Defense Technology (Grant No. 23-ZZCX-JDZ-44).

References

[1] Fang Q N, Xu W S, Chen K K, Wang Y Y, Jiao K, Bai S C, Dai S X and Wang X S 2024 *Opt. Express* **32** 41593
[2] Wang X, Pan J C, Yao C F, Yang Y, Liu Y M, Yang X L, Yang L J and Li P X 2025 *Opt. Lett.* **50** 872
[3] Fu Y L and Zhai T R 2020 *Front. Optoelectron.* **13** 18
[4] Timmerkamp M, Gao M and Fallnich C 2025 *Opt. Express* **33** 8545
[5] Buck S, Oliveira P, Angelides T and Galimberti M 2024 *Photonics* **11** 495
[6] Ding S, Zhang Q, Liu W, Luo J and Sun D 2017 *Front. Optoelectron.* **10** 111
[7] Ye Q, Kong H, Bian J T, Yao J Y, Wang E L, Wu Y, Xu H P, Wen K H and Hu Y H 2023 *Front. Optoelectron.* **16** 26
[8] Guo L Y, Li W F, Qi F, Zhang X Y, Yao J Y, Guo X and Liu P 2025 *Opt. Lett.* **50** 1565
[9] Yao J Y, Mei D J, Bai L, Lin Z S, Yin W L, Fu P Z and Wu Y C 2010 *Inorg. Chem.* **49** 9212
[10] Yang F, Yao J Y, Xu H Y, Feng K, Yin W L, Li F Q, Yang J, Du S F, Peng Q J and Zhang J Y 2013 *Opt. Lett.* **38** 3903
[11] Kostyukova N, Boyko, Baikov D, Shevyrdyaeva G, Panyutin V, Marchev G, Kolker D and Petrov V 2016 *Opt. Lett.* **41** 3667
[12] Kang M Q, Deng Y, Yan X W, Zeng X M, Guo Y W, Yao J Y, Zeng F, Zheng J G, Zhou K N, Qu C B, Shu J Q and Zhu Q H 2019 *Chin. Opt. Lett.* **17** 121402
[13] Bian J T, Yao J Y, Ye Q, Sun X Q, and Kong H 2021 *Chin. Opt. Lett.* **19** 021901
[14] Liu Y, Li Z Y, Yao J Y, Wang H, Zhu Z R, Bai J Z, Fu J J, Lu Y, Zheng Y J, Tan R Q, Ke C J and Yuan H R 2024 *Opt. Lett.* **49** 3255
[15] Hu Z X, Gu X B, Yao J Y, Yuan P, Zhang D F, Wang J, Xie G Q, Qian L J and Ma J G 2025 *Opt. Lett.* **50** 916
[16] Kato K, Miyata K, Badikov V and Petrov V 2018 *Appl. Opt.* **57** 2935
[17] Kato K, Miyata K and Petrov V 2023 *Opt. Mater. Express* **13** 1852
[18] Chen K, Xu D G, Sun Y, Li J N, Yan C, Liu S, Wang Y Y, Zhong K, Yao J Y and Yao J Q 2024 *Opt. Laser Technol.* **171** 110455
[19] Yao J Y, Yin W L, Feng K, Li X M, Mei D J, Lu Q M, Li Y B, Zhang Z W, Hu Z G and Wu Y C 2012 *J. Cryst. Growth* **346** 1